Intersubband transitions in InGaAsN/GaAs quantum wells

Liu, W.; Hou, X. Y.; Jiang, Z. M.; Zhang, Dao Hua; Fan, Weijun

2008

Liu, W., Zhang, D. H., Fan, W., Hou, X. Y.,& Jiang, Z. M. (2008). Intersubband transitions in InGaAsN/GaAs quantum wells. Journal of applied physics, 104, 053119.

https://hdl.handle.net/10356/100808

https://doi.org/10.1063/1.2976335

Intersubband transitions in InGaAsN/GaAs quantum wells

W. Liu,[1] D. H. Zhang,[1,a)] W. J. Fan,[1] X. Y. Hou,[2] and Z. M. Jiang[2]
[1]*School of Electrical and Electronic Engineering, Nanyang Technological University, Singapore 639798, Singapore*
[2]*Department of Physics, Fudan University, People's Republic of China*

(Received 22 April 2008; accepted 7 July 2008; published online 9 September 2008)

The dependences of intersubband transitions on well width and nitrogen (N) content in *n*-type $In_{0.23}Ga_{0.77}As_{1-x}N_x/GaAs$ quantum wells (QWs) are investigated using a ten-band $\mathbf{k}\cdot\mathbf{p}$ model. The absorption peak energy is found to increase first with the well width starting from 2 nm. It becomes insensitive from about 2.5 to 4.5 nm although the absorption intensity increases and bandwidth decreases monotonically, and then keeps decreasing with the well width beyond 4.5 nm. The peak energy is much larger than that of the N-free structure for narrower wells, but the difference decreases quickly with increasing well width. In the case of wider wells, the absorption peak energy shows relatively slow monotonic increase with increasing N content up to 3% because of the N-band and conduction-band coupling. In the nearly lattice-matched GaAsN/AlGaAs QWs the absorption peak energy shows a redshift with increasing N content from 0% to 0.4% and then increases gradually. The theoretical results are consistent with the reported experimental data. © *2008 American Institute of Physics*. [DOI: 10.1063/1.2976335]

I. INTRODUCTION

The InGaAsN alloy has attracted considerable attention in recent years owing to the unique nitrogen (N)-driving physical properties and possible applications for optoelectronic devices.[1–4] It has been found that the incorporation of a small amount of N into (In,Ga)As can cause a significant decrease in the energy band gap and increase in the electron effective mass.[5,6] These are attributed to the highly localized nature of perturbations induced by N although the exact physical mechanism behind them remains the subject of ongoing debates.[7–10] With the $In_xGa_{1-x}As_yN_{1-y}$ alloys, lasers emitting at the 1.3 and 1.5 μm ranges have been demonstrated, which make optical communication accessible to GaAs-based devices[1–3] and solar cells with internal quantum efficiencies of >70% have also been successfully fabricated.[4]

The dilute N materials can also be used for intersubband transition (ISBT) based optoelectronics. With increasing N composition *x*, the $In_{1-y}Ga_yAs_{1-x}N_x/(Al,Ga)As$ QWs can allow the photons with much shorter wavelengths to be absorbed through ISBTs compared to the $In_{1-y}Ga_yAs/(Al,Ga)As$ structure due to the much larger conduction-band discontinuity. On the one hand, this blueshifted absorption enables flexible IR detecting ability without introducing too much indium (In) in the well or using aluminum (Al) in the barrier. On the other hand, the introduction of N can compensate the lattice mismatch caused by In. Indeed, a number of investigations concerning ISBTs in the conduction band (CB) of dilute N-containing QWs have been reported recently.[11–16] For example, Duboz *et al.*[11] reported the observation of ISBTs in *n*-type InGaAsN/GaAs multiple quantum wells (MQWs) for the first time. Luna *et al.*[12] demonstrated double-barrier GaAsN/AlAs/AlGaAs QW infrared photodetector operating in the near infrared. Giehler *et al.*[14] studied the influence of N on the ISBT absorption spectra in (In,Ga)AsN/(Al,Ga)As MQWs and observed an unexpected redshift of main absorption band with increasing N content up to 4%. Liu *et al.*[15] measured the ISBTs in a set of $In_{0.77}Ga_{0.23}As_{0.99}N_{0.01}/GaAs$ MQWs with narrow well widths and found that the transition energy was very insensitive to the well width. Compared with the experimental investigation, only limited theoretical work has been done for the ISBTs in the dilute N-containing QWs.[14–16] The theoretical analyses were mostly based on simplified two-band, three-band $\mathbf{k}\cdot\mathbf{p}$ or analytical models based on band-anticrossing (BAC) theory.

In this paper, we report an investigation of the ISBTs in $In_{1-y}Ga_yAs_{1-x}N_x/(Al,Ga)As$ QWs using a ten-band $\mathbf{k}\cdot\mathbf{p}$ model. The variations of subband dispersions and intersubband absorptions with well width and N content are studied in detail and the theoretical results of the ISBTs are compared with available experimental data.

II. THEORETICAL METHOD

In the ten-band scheme, the total wave function of the subband *n* in the QW can be written as

$$\Psi_n(r) = \sum_{j=1}^{10} F_{n,j}(r)u_j(r), \tag{1}$$

where $F_j(r)$ is the envelope function, $u_j(r)$ is the periodic part of the Bloch basis function at the zone center, $k_t = (k_x, k_y)$ is the two-dimensional in-plane wave vector, and $\rho = (x, y)$ is the two-dimensional in-plane space vector.

The Block basic functions for the high-lying N band (NB), the CB, and the heavy hole (HH), light hole (LH), and spin-orbit split-off (SO) bands we used to derive the Hamiltonian are as follows:

a)Electronic mail: edhzhang@ntu.edu.sg.

$$u_1 = \phi_{\mathrm{NB},\alpha} = |S_N\uparrow\rangle,$$

$$u_2 = \phi_{\mathrm{NB},\beta} = |S_N\downarrow\rangle,$$

$$u_3 = \phi_{\mathrm{CB},\alpha} = |S\uparrow\rangle,$$

$$u_4 = \phi_{\mathrm{CB},\beta} = |S\downarrow\rangle,$$

$$u_5 = \phi_{\mathrm{HH}} = -i\sqrt{1/2}|(X_v + iY_v)\uparrow\rangle,$$

$$u_6 = \phi_{\mathrm{LH},\alpha} = i\sqrt{2/3}|Z_v\uparrow\rangle - i\sqrt{1/6}|(X_v + iY_v)\downarrow\rangle,$$

$$u_7 = \phi_{\mathrm{LH},\beta} = i\sqrt{2/3}|Z_v\downarrow\rangle + i\sqrt{1/6}|(X_v - iY_v)\uparrow\rangle,$$

$$u_8 = \phi_{\mathrm{HH},\beta} = i\sqrt{1/2}|(X_v - iY_v)\downarrow\rangle,$$

$$u_9 = \phi_{\mathrm{SOH},\alpha} = i\sqrt{1/3}|Z_v\uparrow\rangle + i\sqrt{1/3}|(X_v + iY_v)\downarrow\rangle,$$

$$u_{10} = \phi_{\mathrm{SOH},\beta} = -i\sqrt{1/3}|Z_v\downarrow\rangle + i\sqrt{1/3}|(X_v - iY_v)\uparrow\rangle, \tag{2}$$

where $|S\rangle$ denotes the s-like CB Bloch state, $|S_N\rangle$ denotes the s-like NB Bloch state, and $|X_v\rangle$, $|Y_v\rangle$, and $|Z_v\rangle$ denote the p-like VB Bloch states.

The momentum matrix elements P_0 and P_N are defined as

$$P_0 = i\langle S|\mathbf{p}_x|X_v\rangle = i\langle S|\mathbf{p}_y|Y_v\rangle = i\langle S|\mathbf{p}_z|Z_v\rangle \tag{3}$$

and

$$P_N = i\langle S_N|\mathbf{p}_x|X_v\rangle = i\langle S_N|\mathbf{p}_y|Y_v\rangle = i\langle S_N|\mathbf{p}_z|Z_v\rangle, \tag{4}$$

respectively.

The envelope-function Fourier expansion is employed here to calculate the eigenstates and eigenfunctions in the QWs.[17,18] The expansion takes the form of

$$F_{n,j}(r) = \exp[i(k_x x + k_y y)]\sum_m a_{n,j,m}\phi_m(z), \tag{5}$$

where

$$\phi_m(z) = \frac{1}{\sqrt{L}}\exp\left[i\left(k_z + m\frac{2\pi}{L}\right)z\right], \tag{6}$$

where m is a set of integers and L is the sum of the well and barrier widths. Substituting Eq. (5) into the coupled differential equations of

$$\sum_{j'=1}^{10}(H_{j,j'} + U(z)\delta_{j,j'})F_{j'}(r) = EF_j(r), \tag{7}$$

where $U(z)$ is the electronic potential function and $H_{j,j'}$ is the ten-band $\mathbf{k}\cdot\mathbf{p}$ Hamiltonian whose details are listed in the Appendix, then multiplying by $\phi_m^*(z)$ and integrating over L, one gets

$$\sum_{j',m'} H_{j,j'}(m,m')a_{j',m'} = Ea_{j,m}, \quad j,j' = 1,\ldots,10, \tag{8}$$

where the matrix elements $H_{j,j'}(m',m)$ are given by

$$H_{j,j'}(m,m') = \int_{-L/2}^{L/2}\phi_m^*(z)[H_{j,j'} + \delta_{j,j'}U(z)]\phi_{m'}(z)dz$$
$$= \langle\phi_m|H_{j,j'} + \delta_{j,j'}U(z)|\phi_{m'}\rangle. \tag{9}$$

The electronic potential function $U(z)$ in Eq. (11) consists of two parts. One is the QW potential from the band discontinuity between the well and barrier and the other is the strain-induced potential change.

The following probability functions are introduced to determine the NB, CB, HH, LH, and SO components in the QW eigenstates:

$$P_n^{\mathrm{NB}} = \sum_{j=1,2}\sum_m a_{n,j,m}^* a_{n,j,m} P_n^{\mathrm{CB}} = \sum_{j=3,4}\sum_m a_{n,j,m}^* a_{n,j,m},$$

$$P_n^{\mathrm{HH}} = \sum_{j=5,8}\sum_m a_{n,j,m}^* a_{n,j,m}, \quad P_n^{\mathrm{LH}} = \sum_{j=6,7}\sum_m a_{n,j,m}^* a_{n,j,m},$$

$$P_n^{\mathrm{SO}} = \sum_{j=9,10}\sum_m a_{n,j,m}^* a_{n,j,m}. \tag{10}$$

These probability functions are particularly useful in identifying the dominant character in a particular subband. Note that the following sum rule should hold:

$$\sum_i P_n^i = 1, \quad i = \mathrm{NB,CB,HH,LH,SO}. \tag{11}$$

The momentum matrix element between subband n and n' is

$$M_{n,n'} = \langle\Psi_n|e_v\cdot\mathbf{p}|\ \ \Psi_{n'}\rangle = \sum_{j,j'=1}^{10}\langle F_{n,j}u_j|e_v\cdot\mathbf{p}|\ \ F_{n',j'}u_{j'}\rangle, \tag{12}$$

where $\mathbf{p}$ is the momentum operator and $e_v = \nu_x e_x + \nu_y e_y + \nu_z e_z (\nu_x^2 + \nu_y^2 + \nu_z^2 = 1)$ is the photon polarization unit vector. Substituting Eqs. (2) and (5) into Eq. (12), we obtain

$$M_{n,n'} = \sum_{j,j'=1}^{10}\left\langle\sum_m a_{n,j,m}\phi_m(z)u_j\middle|e_v\cdot\mathbf{p}\middle|\sum_{m'}a_{n',j',m'}\phi_{m'}(z)u_{j'}\right\rangle$$
$$\approx \sum_{j,j'=1}^{10}\left[\left\langle\sum_m a_{n,j,m}\phi_m(z)\middle|e_v\cdot\mathbf{p}\middle|\sum_{m'}a_{n',j',m'}\phi_{m'}(z)\right\rangle \times\langle u_j|u_{j'}\rangle\right]$$
$$+ \sum_{j,j'=1}^{10}\left[\left\langle\sum_m a_{n,j,m}\phi_m(z)\middle|\sum_{m'}a_{n',j',m'}\phi_{m'}(z)\right\rangle \times\langle u_j|e_v\cdot\mathbf{p}|u_{j'}\rangle\right]$$
$$= \sum_{j=1}^{8}\left[\left\langle\sum_m a_{n,j,m}\phi_m(z)\middle|e_v\cdot\mathbf{p}\middle|\sum_{m'}a_{n',j,m'}\phi_{m'}(z)\right\rangle\right]$$
$$+ \sum_{j,j'=1}^{8}\left[\sum_m (a_{n,j,m}^*\cdot a_{n',j',m})\langle u_j|e_v\cdot\mathbf{p}|u_{j'}\rangle\right], \tag{13}$$

where the first term on the right of Eq. (13) represents the

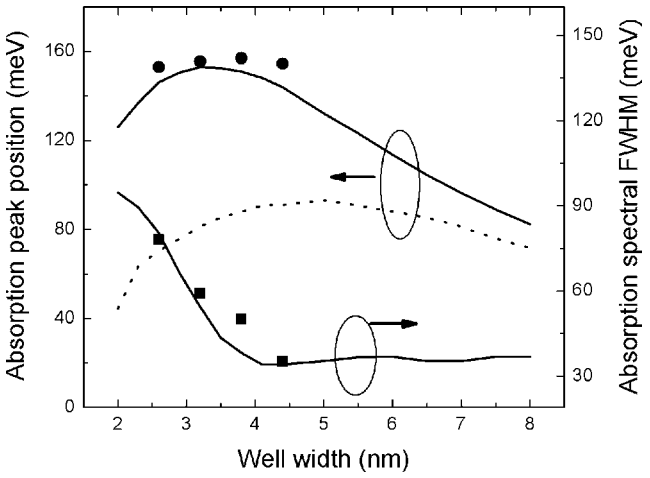

FIG. 1. Calculated absorption peak energy and spectral FWHM as a function of well width for the $In_{0.23}Ga_{0.77}As_{0.99}N_{0.01}/GaAs$ QW. The solid curves are calculated results, and the solid squares and circles are the experimental data from Ref. 15. The dash curve shows the absorption peak energy of N-free $In_{0.23}Ga_{0.77}As/GaAs$ QW.

transitions within the same Bloch basis states (intraband contribution), and the second term represents the transitions between $|S\rangle$ and $|v\rangle$ ($|v\rangle=|X_v\rangle$, $|Y_v\rangle$, or $|Z_v\rangle$) states (interband contribution).

With the momentum matrix element of respective ISBT worked out, the relative optical absorption coefficient can be calculated by[19]

$$\alpha_{n,n'}(\hbar\omega) = \frac{\pi e^2}{n_r c\varepsilon_0 m_0^2 \omega}\frac{2}{V}\sum_{k_t}|M_{n,n'}|^2(f_n - f_{n'}),$$

$$(\Gamma/2\pi)/[(E_{n'} - E_n - \hbar\omega)^2 + (\Gamma/2)^2], \qquad (14)$$

where f_n and $f_{n'}$ are the Fermi–Dirac distributions for electrons in respective subbands, k_t is the in-plane wave vector, Γ is an dephasing rate in the Lorentzian line shape to interpret the homogeneous broadening, e is the electron charge, ε_0 is the free-space dielectric constant, n_r is the refractive index, V is the space volume, and ω is the photon frequency.

One ideal approach to compute the optical material gain and absorption properties of the semiconductor quantum systems is the fully microscopic many-body model that yields excellent agreement with experiments for the QW lasers which are based on interband transitions.[20–22] For the ISBTs within the CB, the absorption coefficient spectra are usually calculated by considering the momentum matrix element, subband energy, Fermi occupation factor, and scattering related line broadening with an effective dephasing rate.[19,23–25] In recent years, the microscope theory based on self-consistent field approach, the Green's function, or the density matrix formalism has been developed to study the many-body effects on the intersubband absorptions.[26–30] Such effects like Coulomb interaction induced collective excitations and phase space filling are found to significantly affect the absorption peak position and shape for the heavily doped (generally $\sim 10^{19}$ cm^{-3} or above) QWs. For the QWs with lower doping concentration, however, the many-body effects are not significant, and the intersubband absorption is found to be close to that of the free-carrier case.[26,28–30] As we are studying the QWs with a doping level of about 1×10^{18} cm^{-3}, the many-body effects on the optical absorption should not be significant.

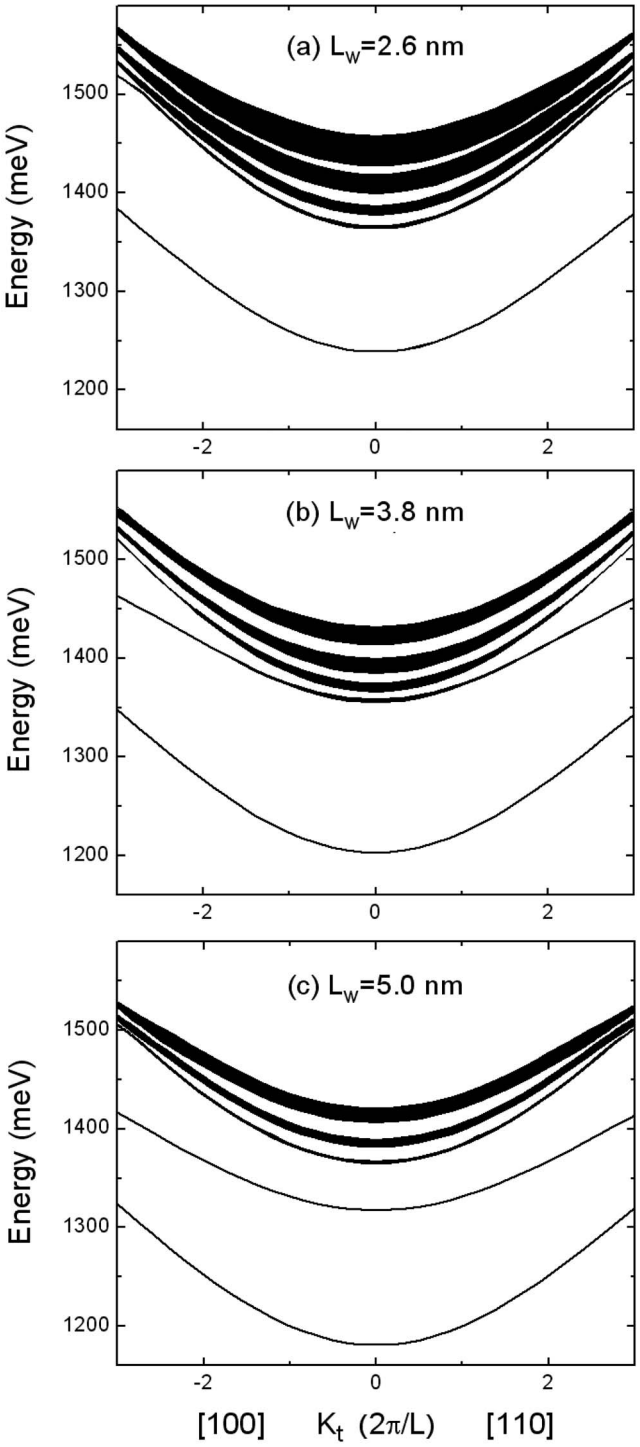

FIG. 2. Dispersions of conduction subbands as a function of k_t along the [100] and [110] directions in the $In_{0.23}Ga_{0.77}As_{0.99}N_{0.01}/GaAs$ QWs with well widths of (a) 2.6 nm, (b) 3.8 nm, and (c) 5.0 nm. The bulk VB edge of $In_{0.23}Ga_{0.77}As$ is taken as zero energy.

III. RESULTS AND DISCUSSION

A. Variation of ISBTs with well width

The structures analyzed are $In_{0.23}Ga_{0.77}As_{0.99}N_{0.01}/GaAs$ *n*-type MQWs, which enable us to directly compare the the-

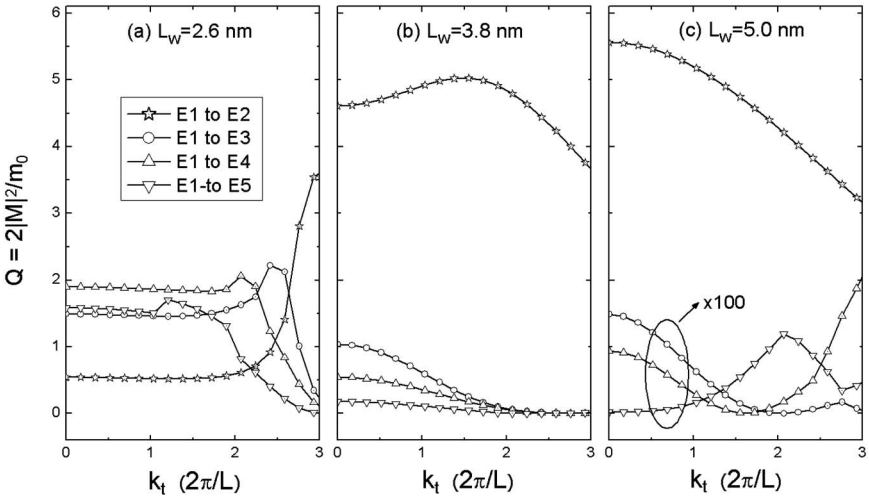

FIG. 3. Calculated squared optical transition matrix elements (TM polarization) as a function of k_t along the [110] direction for E1 to E2–E5 transitions in the $In_{0.23}Ga_{0.77}As_{0.99}N_{0.01}$/GaAs QWs with well widths of (a) 2.6 nm, (b) 3.8 nm, and (c) 5.0 nm, respectively. "×100" indicates that the curve shown is one hundred times of the real data.

oretical results with the reported experimental observations.[15] The CB offset ratio between the InGaAsN well and the GaAs barrier is assumed to be 0.8.[31] The GaAs barrier width is assumed to be 20 nm. The *n*-doping concentration N_D in wells is assumed to be 1×10^{18} cm^{-3}. In the calculation the basic III-V material parameters of binary and ternary compound semiconductors for room temperature were taken from Refs. 32 and 33. The values of two important N-related parameters in matrix (1), E_{N0} and β, are taken from Ref. 6. The coupling between NB and VB is regarded as neglectable.[33] The Lorentzian linewidth Γ in Eq. (14) is assumed to be 28 meV.[19]

Figure 1 shows the calculated transition energy at absorption peak and the spectrum full width at half maximum (FWHM) as a function of well width (L_W), which ranged from 2 to 8 nm. The experimental data from Ref. 15 are also marked with solid dots and squares. In addition, the calculated absorption peak energies for N-free $In_{0.23}Ga_{0.77}As$/GaAs QWs are shown in Fig. 1 with a dash curve for comparison. In the calculation the transitions from the ground state (E1) to the first four excited states (E2–E5) for normal-to-plane (TM) polarization are taken into consideration. We can see that the absorption peak of the InGaAsN/GaAs QW exhibits a blueshift first with increasing well width from 2 to 3.5 nm. The absorption spectrum FWHM appears broad due to the superposition of comparable ground to continuum state transitions. When L_W is over 3.5 nm, the transition energy tends to decrease as the first excited state (E2) begins to move downward quickly. At the same time the absorption spectrum FWHM becomes narrow as the E1 to E2 transition becomes dominating.

To look into the ISBT details in the N-containing structures clearly, we plot the calculated energy dispersions of subbands, the squared optical transition matrix elements, and the optical absorption spectra of ISBTs in Figs. 2–4, respectively, for well widths of 2.6, 3.8, and 5.0 nm. The squared optical transition matrix element $Q_{n,n'}=2|M_{n,n'}|^2/m_0$ is an indicator of transition rates between the ground and excited levels. In Fig. 2 the lowest five conduction subbands (E1–E5) are shown. It can be seen that the higher excited states appear as minibands because of the relaxation of quantum confinement in the QW growth direction. The subbands move downward gradually with increasing well width and the minibandwidths also decrease. In the case of a 2.6 nm wide well, all the excited levels are continuum states due to the very narrow well width. The bound-to-continuum (B-to-C) transitions from E1 to E2–E5 have comparable rates as shown in Fig. 3(a). The superposition of comparable E1 to E2–E5 absorptions results in a broad overall absorption spectrum as shown in Fig. 4(a). The spectral FWHM is 80.5 meV

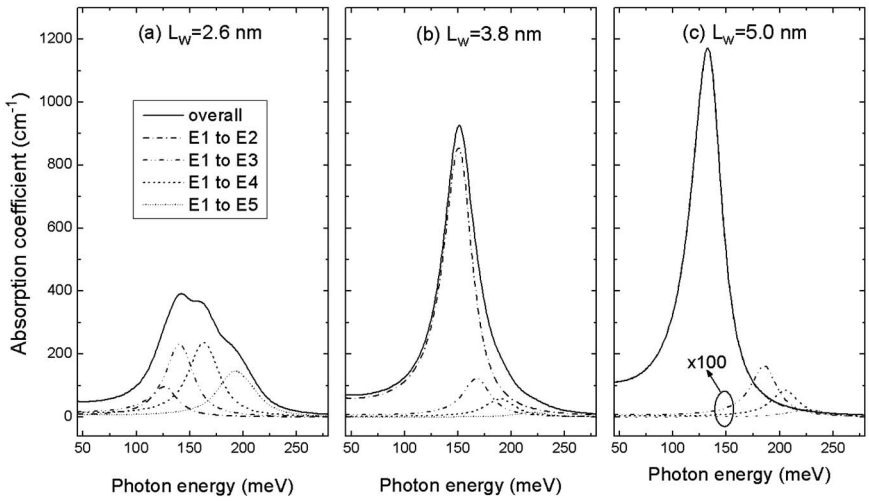

FIG. 4. Calculated optical absorption coefficient spectra for well widths of (a) 2.6 nm, (b) 3.8 nm, and (d) 5.0 nm, respectively. The solid curve is the overall absorption and the dash curves are the respective intersubband absorptions.

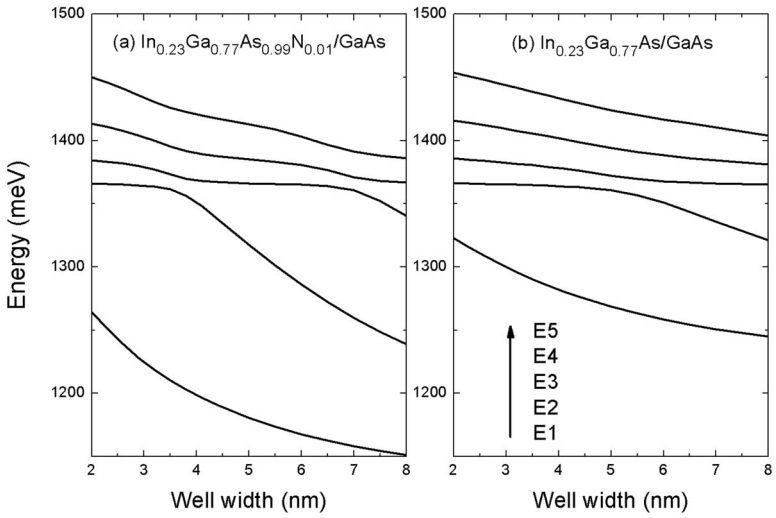

FIG. 5. Calculated subbands energies at $k_t=0$ as a function of well width for the N-containing QW and equivalent N-free QW.

and the absorption peak energy is 146.1 meV. When the well width increases to 3.8 nm, E2 turns to a quasibound state and the E1 to E2 transition rate is obviously larger than the others as shown in Fig. 3(b). Consequently, the FWHM of overall absorption spectrum narrows to about 54.5 meV as shown in Fig. 4(b). The absorption peak energy is 151.1 meV, which is decided mainly by the E1 to E2 transition. When the well width increases further to 5.0 nm, E2 goes down quickly to become a completely bound state as shown in Fig. 2(c). The E1 to E2 transition is dominant and the other transitions have negligible rates. The overall absorption spectrum becomes very narrow since it is completely dominated by the E1 to E2 transition as shown in Fig. 4(c). The spectral FWHM is only about 34.1 meV and the transition energy at the absorption peak decreases to 132.3 meV due to the large lowering of E2 level. The calculated peak absorption coefficients are 392.3, 927.2, and 1171.6 cm^{-1} for well widths of 2.6, 3.8, and 5.0 nm, respectively. It can be seen that in the case of narrower well widths (about 2.5–4.5 nm), the absorption peak energy is relatively insensitive with the increase in well width while the absorption intensity increases and bandwidth decreases greatly, which is consistent with the reported experimental data.[15] In wider wells the absorption peak energy keeps decreasing with the increase in well width because of the continuous lowering of E2.

It is interesting to note that the absorption peak energy of the InGaAsN/GaAs QW is much greater than that of the equivalent N-free QW in the case of narrower well widths (about 2–4.5 nm), but the difference becomes very small in wider wells. To understand the reason, we show in Fig. 5 the energies of subbands E1–E5 at the zone center ($k_t=0$) as a function of well width in the N-containing and N-free QWs. The $In_{0.23}Ga_{0.77}As$ bulk valence-band edge is taken as zero energy. It can be seen that the coupling of NB and CB in InGaAsN results in two significant influences on the subband dispersions. First, the energy level of the ground state E1 in the InGaAsN/GaAs QW is much lower than that in the equivalent N-free structure, and the change of E2 from continuum to bound states occurs at a narrower well width (~3.5 nm) in the former compared to the case in the latter (~5 nm) due to the interaction between NB and CB. Second, the lowering of E1 with increasing well width in the $In_{0.23}Ga_{0.77}As_{0.99}N_{0.01}$ well is much quicker than that in the $In_{0.23}Ga_{0.77}As$ well. This phenomenon also occurs in E2 after it becomes a bound state. For instance, the reduced energies of E1 are 113 meV (from 1264 to 1151 meV) and 78 meV (from 1323 to 1245 meV) for the N-containing and N-free QWs, respectively, when L_W increases from 2 to 8 nm. The reduced energy of bound state E2 is 122 meV (from 1361 to

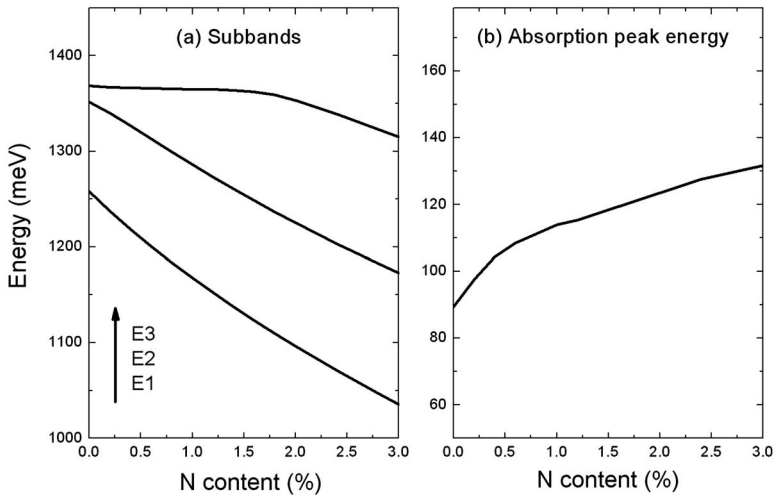

FIG. 6. Calculated (a) energies of subbands E1–E3 at $k_t=0$ and (b) peak position in the overall ISBT absorption as a function of N content (N_N) for the $In_{0.23}Ga_{0.77}As_{1-x}N_x$/GaAs QW.

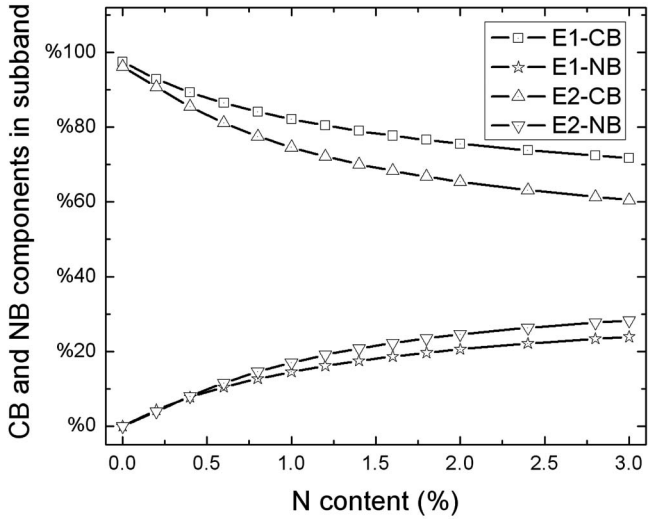

FIG. 7. NB and CB components in E1 and E2 states at $k_t=0$ as a function of N_N in the $In_{0.23}Ga_{0.77}As_{1-x}N_x/GaAs$ QW.

1239 meV) in the N-containing QW when L_W increases from 3.5 to 8 nm, but is only 39 meV (from 1361 to 1322 meV) in the N-free QW when L_W increases from 5 to 8 nm. Consequently, the absorption peak energy in the former can be about 50–80 meV larger than that in the latter for narrower well widths ($L_W<4.5$ nm) since E1 is pushed down evidently due to the interaction of NB and CB. In the wider wells, the N-related effect makes E2 go downward quickly and so the E1 $\rightarrow$E2 transition energy decreases remarkably, which diminishes the difference in absorption peak positions of the equivalent N-containing and N-free QWs.

B. Variation of ISBTs with N content

In this section, the dependence of ISBTs on N content (N_N) will be addressed based on the ten-band $\mathbf{k}\cdot\mathbf{p}$ model. Figure 6 shows the calculated energies of subbands E1–E3 at the zone center ($k_t=0$) and the absorption peak energy in overall absorption spectrum as a function of N_N up to 3% for the $In_{0.23}Ga_{0.77}As_{1-x}N_x/GaAs$ QWs with 6 nm well width. In this structure both E1 and E2 are bound states and the E1 $\rightarrow$E2 transition dominates in the overall intersubband absorption. Therefore, the theoretical absorption peak energy is very close to the energy separation between E1 and E2. It is interesting to find that in the $In_{0.23}Ga_{0.77}As_{1-x}N_x/GaAs$ structure the E1 and E2 energy levels go down with comparable rates as N_N increases, resulting in a relatively small variation of the absorption peak energy. When N_N varies from 0 to 3%, the absorption peak energy only increases from 90 to 130 meV although the 3% N content has increased the well depth by about 200 meV. This is unlike the well known phenomenon in common N-free (In,Ga)As/(Al,Ga)As QWs in which the absorption peak energy increases quickly with the well depth. The cause is that the interaction between NB and CB has comparable repulsion effects on the ground and bound excited states. Figure 7 shows the NB and CB components in the E1 and E2 states at $k_t=0$ as a function of N_N calculated using Eq. (10) in order to examine the intermixing of NB and CB wave functions in the electron states. It can be seen that the NB component in E1 (P_{E1}^{NB}) increases quickly to 14.6% with increasing N_N to 1%, and further to 23.9% at $N_N=3\%$. The NB component in E2 (P_{E2}^{NB}) goes up to 17.1% with increasing N_N to 1.0%, and then reaches 28.3% at $N_N=3\%$. It is clearly shown that the admixing of NB wave function in E1 and E2 states intensifies with the increase in N_N, and the NB admixing in E2 is slightly stronger than that in E1 which indicates that the higher energy subband is more interacted with NB.

Actually this phenomenon should appear more obvious in nearly lattice-matched GaAsN/AlGaAs QWs in which In-induced large compressive strains are absent. Figure 8 shows the calculated subband energies at $k_t=0$ and the absorption peak energy as a function of N_N for a $GaAs_{1-x}N_x/Al_{0.35}Ga_{0.65}As$ structure with 6 nm well width and 20 nm barrier width. The CB offset ratio between the well and the barrier is assumed to be 0.65.[34] We can see that the absorption peak energy shows relatively small variations (within 144–171 meV) with the increase in N_N by up to 3%, although the N incorporation has induced bandgap narrowing with a ratio of approximate 100 meV per 1% N in this structure. Furthermore, it can be seen that the absorption peak energy exhibits a moderate redshift with increasing N_N from 0 to 0.4% and then begins to increase gradually with increasing N_N over 0.5%. This is because the lowering of E2 is

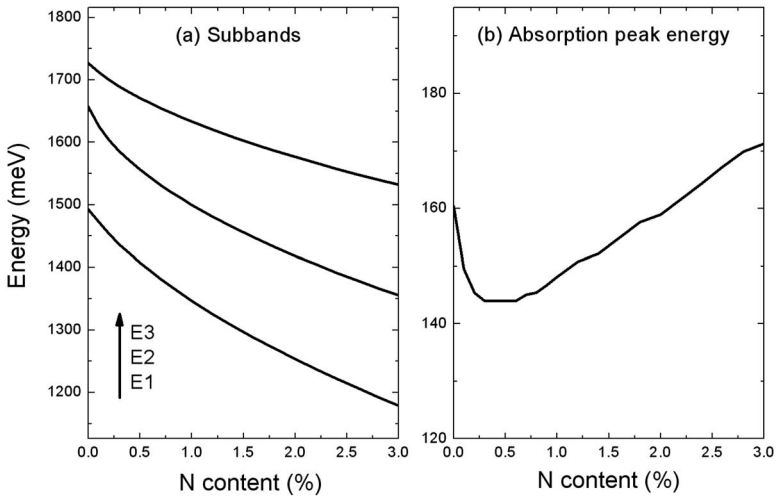

FIG. 8. Calculated (a) energies of subbands E1–E3 at $k_t=0$ and (b) peak position in the overall ISBT absorption as a function of N_N for the $GaAs_{1-x}N_x/Al_{0.35}Ga_{0.65}As$ QW.

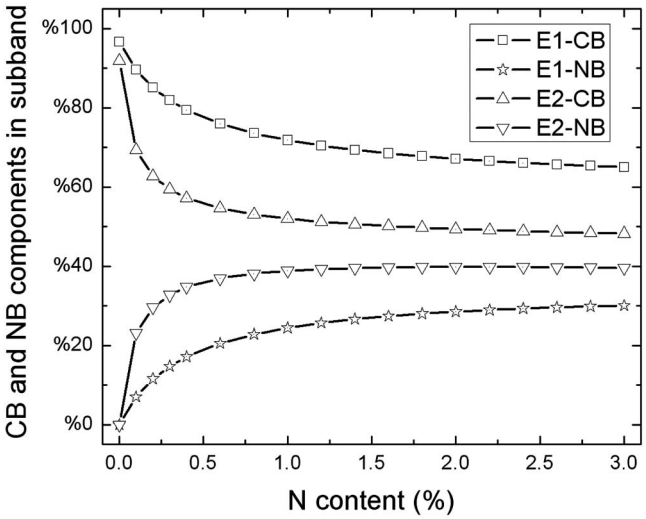

FIG. 9. NB and CB components in E1 and E2 states at $k_t=0$ as a function of N_N for the $GaAs_{1-x}N_x/Al_{0.35}Ga_{0.65}As$ QW.

slightly quicker than that of E1 with increasing N_N as shown in Fig. 8(a). The largest redshift occurs at $N_N \approx 0.4\% - 0.5\%$ and the corresponding absorption peak locates at 144 meV. The absorption peak energies with increasing N_N up to 2.1% are smaller than that (160 meV) for $N_N=0$. The theoretical results are consistent with the measured absorption band redshifts in GaAsN/AlGaAs QWs reported in Ref. 14. The calculated NB and CB components in the E1 and E2 states at $k_t=0$ as a function of N_N are shown in Fig. 9. Compared with the $In_{0.23}Ga_{0.77}As_{1-x}N_x/GaAs$ structure, the $GaAs_{1-x}N_x/Al_{0.35}Ga_{0.65}As$ structure has a larger well depth and has no compressive strain in the well, and therefore the lowering of E2 state in it with the increase in N content is less hindered. This is the reason why a redshift of absorption peak energy can show in the latter.

IV. CONCLUSIONS

In summary, the variations of ISBT and absorption intensity with well width and N content in InGaAsN/GaAs QWs are analyzed in detail using the ten-band $\mathbf{k}\cdot\mathbf{p}$ model. It is found that the absorption peak energy is insensitive to the well width within 2.5–4.5 nm while the absorption intensity increases and the bandwidth decreases greatly with the increase in well width. The absorption peak energy is much larger than that of the N-free structure in narrower wells, but the difference becomes small quickly in wider wells. In the case of wider wells where the transition from E1 to the bound E2 state dominates, the absorption peak energy shows relatively small variations with increasing N content of up to 3% because the NB and CB coupling affects the conduction subbands comparably. The theoretical results show that the dilute N-related physics has made some significant changes to the ISBT properties, which are consistent with reported experiment data. Our work indicates that the BAC-based ten-band $\mathbf{k}\cdot\mathbf{p}$ model can describe well the ISBT properties in dilute N-containing QWs.

APPENDIX: TEN-BAND K·P HALMILTONIAN

The ten-band $\mathbf{k}\cdot\mathbf{p}$ Hamiltonian, which takes the coupling of NB, CB, HH, LH, and SO into account, is given below:

$$
\mathrm{H}_k = \begin{pmatrix}
N & 0 & V_{NC} & 0 & -p_N k_+ & \sqrt{\frac{2}{3}}p_N k_z & \frac{1}{\sqrt{3}}p_N k_- & 0 & \frac{1}{\sqrt{3}}p_N k_z & \sqrt{\frac{2}{3}}p_N k_- \\
0 & N & 0 & V_{Nc} & 0 & \frac{-1}{\sqrt{3}}p_N k_+ & \sqrt{\frac{2}{3}}p_N k_z & p_N k_- & \sqrt{\frac{2}{3}}p_N k_+ & -\frac{1}{\sqrt{3}}p_N k_z \\
\cdots & \cdots & C & 0 & -pk_+ & \sqrt{\frac{2}{3}}pk_z & \frac{1}{\sqrt{3}}pk_- & 0 & \frac{1}{\sqrt{3}}pk_z & \sqrt{\frac{2}{3}}pk_- \\
\cdots & \cdots & \cdots & C & 0 & \frac{-1}{\sqrt{3}}pk_+ & \sqrt{\frac{2}{3}}pk_z & pk_- & \sqrt{\frac{2}{3}}pk_+ & -\frac{1}{\sqrt{3}}pk_z \\
\cdots & \cdots & \cdots & \cdots & F & H & I & 0 & \frac{H}{\sqrt{2}} & \sqrt{2}I \\
\cdots & \cdots & \cdots & \cdots & \cdots & G & 0 & I & \frac{1}{\sqrt{2}}(G-F) & -\sqrt{\frac{3}{2}}H \\
\cdots & \cdots & \cdots & \cdots & \cdots & \cdots & G & -H & -\sqrt{\frac{3}{2}}H^* & \frac{-1}{\sqrt{2}}(G-F) \\
\cdots & \cdots & \cdots & \cdots & \cdots & \cdots & \cdots & F & -\sqrt{2}I^* & \frac{H^*}{\sqrt{2}} \\
\cdots & \cdots & \cdots & \cdots & \cdots & \cdots & \cdots & \cdots & \frac{F+G}{2}-\Delta & 0 \\
\cdots & \cdots & \cdots & \cdots & \cdots & \cdots & \cdots & \cdots & \cdots & \frac{F+G}{2}-\Delta
\end{pmatrix},
$$

where

$$N = E_{N0} + \alpha_N k^2,$$

$$C = E_G + \frac{\hbar^2 k^2}{2m_0}\left[\frac{1}{m_e^*} - \frac{E_P}{3}\left(\frac{2}{E_g} + \frac{1}{E_g + \Delta}\right)\right],$$

$$F = Ak^2 + \frac{B}{2}(k^2 - 3k_z^2), \quad G = Ak^2 - \frac{B}{2}(k^2 - 3k_z^2),$$

$$H = -Dk_z(k_x - ik_y), \quad I = -\frac{\sqrt{3}}{2}B(k_x^2 - k_y^2) + iDk_xk_y,$$

$$A = -\frac{\hbar^2\gamma_1}{2m_0}, \quad B = -\frac{\hbar^2\gamma_2}{m_0}, \quad D = -\sqrt{3}\frac{\hbar^2\gamma_3}{m_0},$$

$$k_+ = (k_x + ik_y)/\sqrt{2}, \quad k_- = (k_x - ik_y)/\sqrt{2},$$

$$p = (\hbar/m_0)P_0, \quad p_N = (\hbar/m_0)P_N,$$

and

$$V_{NC} = \beta\sqrt{x},$$

where E_{N0} and E_G are the energies of NB and CB, respectively, Δ is the spin-orbit splitting energy, k_x and k_y are the wave vectors in the plane, k_z is the wave vector along the QW growth direction, γ_1, γ_2, and γ_3 are the modified Luttinger parameters, β is the interaction factor between NB and CB, and x is the N content. The down triangular block in the Hamiltonian matrix is not shown since it is Hermitian. The strain Hamiltonian H_s can be derived by the following substitution because of the same underlying symmetry: $A \rightarrow a_v$, $B \rightarrow b$, $D \rightarrow d$, $k_\alpha k_\beta \rightarrow \varepsilon_{\alpha\beta}$ $(\alpha, \beta = x, y, z)$, and $\hbar^2k^2/2m_0 \leftrightarrow a_c$ for CB, where $\varepsilon_{\alpha\beta}$ is the strain tensor, b and d are the shear deformation potentials, a_v is the hydrostatic valence-band deformation potential, and a_c is the conduction-band deformation potential.

[1] M. Kondow, K. Uomi, A. Niwa, T. Kitatani, S. Watahiki, and Y. Yazawa, Jpn. J. Appl. Phys., Part 1 **35**, 1273 (1996).
[2] T. Miyamoto, K. Takeuchi, F. Koyama, and K. Iga, IEEE Photonics Technol. Lett. **9**, 1448 (1997).
[3] M. Hetterich, M. D. Dawson, A. Yu. Egorov, D. Bernklau, and H. Riechert, Appl. Phys. Lett. **76**, 1030 (2000).
[4] S. R. Kurtz, A. A. Allerman, E. D. Jones, J. M. Gee, J. J. Banas, and B. E. Hammons, Appl. Phys. Lett. **74**, 729 (1999).
[5] M. Weyers, M. Sato, and H. Ando, Jpn. J. Appl. Phys., Part 2 **31**, L853 (1992).
[6] J.-Y. Duboz, J. A. Gupta, Z. R. Wasilewski, J. Ramsey, R. L. Williams, G. C. Aers, B. J. Riel, and G. I. Sproule, Phys. Rev. B **66**, 085313 (2002).
[7] W. Shan, W. Walukiewicz, J. W. Ager, E. E. Haller, J. F. Geisz, D. J. Friedman, J. M. Olson, and S. R. Kurtz, Phys. Rev. Lett. **82**, 1221 (1999).
[8] J. D. Perkins, A. Mascarenhas, Y. Zhang, J. F. Geisz, D. J. Friedman, J. M. Olson, and S. R. Kurtz, Phys. Rev. Lett. **82**, 3312 (1999).
[9] E. D. Jones, N. A. Modine, A. A. Allerman, S. R. Kurtz, A. F. Wright, S. T. Torez, and X. Wei, Phys. Rev. B **60**, 4430 (1999).
[10] T. Mattila, S.-H. Wei, and A. Zunger, Phys. Rev. B **60**, R11245 (1999).
[11] J.-Y. Duboz, J. A. Gupta, M. Byloss, G. C. Aers, H. C. Liu, and Z. R. Wasilewski, Appl. Phys. Lett. **81**, 1836 (2002).
[12] E. Luna, M. Hopkinson, J. M. Ulloa, A. Guzmán, and E. Muñoz, Appl. Phys. Lett. **83**, 3111 (2003).
[13] D. H. Zhang, W. Liu, L. Sun, W. J. Fan, S. F. Yoon, S. Z. Wang, and H. C. Liu, J. Appl. Phys. **99**, 043514 (2006).
[14] M. Giehler, R. Hey, P. Kleinert, and H. T. Grahn, Phys. Rev. B **73**, 085322 (2006).
[15] H. C. Liu, C. Y. Song, J. A. Gupta, and G. C. Aers, Appl. Phys. Lett. **89**, 241122 (2006).
[16] J.-Y. Duboz, Phys. Rev. B **75**, 045327 (2007).
[17] J.-B. Xia and W.-J. Fan, Phys. Rev. B **40**, 8508 (1989).
[18] W. J. Fan and S. F. Yoon, J. Appl. Phys. **90**, 843 (2001).
[19] S. L. Chuang, in *Physics of Optoelectronic Devices*, Wiley Series in Pure and Applied Optics, edited by J. W. Goodman (Wiley, New York, 1995), Chap. 9.
[20] J. Hader, J. V. Moloney, S. W. Koch, and W. W. Chow, IEEE J. Sel. Top. Quantum Electron. **9**, 688 (2003).
[21] J. Hader, J. V. Moloney, and S. W. Koch, Proc. SPIE **6115**, 61151T (2006).
[22] J. Hader, J. V. Moloney, E. P. O'Reilley, and M. R. Hofmann, Proc. SPIE **4283**, 36 (2001).
[23] M. E. Flatté, P. M. Young, L.-H. Peng, and H. Ehrenreich, Phys. Rev. B **53**, 1963 (1996).
[24] C. W. Cheah, L. S. Tan, and G. Karunasiri, J. Appl. Phys. **91**, 5105 (2002).
[25] W. Liu, D. H. Zhang, Z. M. Huang, and W. J. Fan, J. Appl. Phys. **101**, 033114 (2007).
[26] D. Huang, G. Gumbs, and M. O. Manasreh, Phys. Rev. B **52**, 14126 (1995).
[27] D. E. Nikonov, A. Imamoğlu, L. V. Butov, and H. Schmidt, Phys. Rev. Lett. **79**, 4633 (1997).
[28] K.-Y. Kim, B. Lee, and C. Lee, IEEE J. Quantum Electron. **35**, 1491 (1999).
[29] J. Li and C. Z. Ning, Phys. Rev. Lett. **91**, 097401 (2003).
[30] J. Li and C. Z. Ning, Proc. SPIE **5349**, 95 (2004).
[31] Z. Pan, L. H. Li, Y. W. Lin, B. Q. Sun, and D. S. Jiang, Appl. Phys. Lett. **78**, 2217 (2001).
[32] I. Vurgaftman, J. R. Meyer, and L. R. Ram-Mohan, J. Appl. Phys. **89**, 5815 (2001).
[33] E. P. O'Reilly, A. Lindsay, S. Tomić, and M. Kamal-Saadi, Semicond. Sci. Technol. **17**, 870 (2002).
[34] D. J. Arent, Phys. Rev. B **41**, 9843 (1990).